ELSEVIER

Journal of Molecular Catalysis A: Chemical 129 (1998) 297–310

JOURNAL OF MOLECULAR CATALYSIS A: CHEMICAL

Methane oxidation reactions on $MoO_3(100)$: A theoretical study

B. Irigoyen [a,*], N. Castellani [a,b], A. Juan [a,1]

[a] *Departamento de Física, Universidad Nacional del Sur, Avda. Alem 1253, 8000 Bahia Blanca, Argentina*
[b] *Planta Piloto de Ingeniería Química, UNS-CONICET, 12 de Octubre 1842, 8000 Bahia Blanca, Argentina*

Received 2 May 1997

Abstract

A molecular orbital study of methane oxidation reactions on the (100) surface of MoO_3 is made. The adsorption energy for the molecular species or fragments has been computed using a methodology based on the atom superposition and electron delocalization molecular orbital (ASED-MO) theory. Calculations were performed using a bulk superimposable $Mo_{30}O_{107}^{-34}$ cluster model. Different sequences and sites for H abstraction from methane were explored on layers exposing molybdenum or oxygen atoms. The oxygen coordination and the geometric arrangements for the adsorbed species were analyzed. The process appears to be endothermic. The formation of oxygenated products such as formaldehyde, CO and CO_2 is also addressed. Our results are in good agreement with recent literature reports, showing that total oxidation of methane is difficult to achieve. © 1998 Elsevier Science B.V.

Keywords: Methane oxidation; Molybdenum oxide; ASED-MO; Oxidation catalysts

1. Introduction

Methane is the major component of natural gas, often constituting more than 90% of the hydrocarbon fraction of the gas. The functionalisation of methane for manufacturing valuable products is of great importance. Since partial oxidation is one of the main processes used to functionalise hydrocarbon molecules, several researchers have intensified the investigation of the conversion of methane to higher hydrocarbons by partial oxidation and oxidative coupling [1].

The global reaction for the catalyzed oxidation of methane can be written as:

$$mCH_4 + nO_2 \rightarrow pC_2H_6 + qC_2H_4 + rCO_x + sH_2O$$

Reactions of catalytic oxidation may be divided into two categories: (1) electrophilic oxidation, proceeding through the activation of oxygen and (2) nucleophilic oxidation, in which activation of the hydrocarbon molecule is the first step followed by consecutive steps of nucleophilic oxygen insertion and hydrogen abstraction. In each of these processes the carbon skeleton remains unchanged [2].

The oxidative coupling of methane (OCM) has been proposed as an alternative for the chemical utilization of natural gas. Catalysts used for the OCM are usually composed of

* Corresponding author. Fax: +54-91-883933; e-mail: cajuan@criba.edu.ar
[1] Present address: Department of Chemistry, Cornell University, Ithaca 14853, USA. E-mail: aj29@cornell.edu

PII S1381-1169(97)00192-1

metal oxides. The oxygen species on the catalyst surface (either surface lattice oxygen or adsorbed oxygen) interact with methane, leading to formation of methyl species. Subsequent coupling of methyl species results in ethane and, by its dehydrogenation, in ethylene. Methyl radicals as well as C_2 hydrocarbons in their radical form may also interact with surface and gas-phase oxygen leading to total oxidation [3]. An exhaustive review for the OCM has been recently published [4].

The rate-determining step in the selective oxidation of methane is the rupture of the C–H bond. There are two main hypotheses on this subject under discussion.

According to Ito and Lunsford methane activation occurs by a homolytic mechanism [5]:

$$\text{Cat-}[O^-] + CH_4 \rightarrow \text{Cat-OH} + CH_3^{\cdot}$$

This first hypothesis has been substantiated by the presence of methyl radicals on the surface of the MgO catalyst, as reported in Ref. [6]. The methyl radicals so formed on the surface could react with the catalyst and produce methoxide ions, which on a subsequent reaction with water yield methanol. Further oxidation of methanol or dehydrogenation of methoxide ion leads to the formation of formaldehyde.

The second hypothesis has been recently proposed by Sokolovskii and co-workers. They suggested that the methane activation proceeds heterolytically via its interaction with an acid–base pair, giving place to a proton detachment and the formation of a metal–methyl compound, where the methyl results in being negatively charged [7]:

$$Me^{+2}O^{-2} + CH_4 \rightarrow CH_3^- Me^{+2} + H^+O^{-2}$$

The coordinately unsaturated metal ion paired with a strong nucleophile (O^{-2} ion) may act as an active center [8].

Further oxidation of these surface methyl anions would lead to methyl radicals, which then dimerize:

$$CH_3^- Me^{+2} \rightarrow CH_3^{\cdot} + Me^{+2} + e^-$$

In contrast with the considerable amount of papers published about the activation of methane on pure transition metals, the theoretical studies of this reaction on metal oxides have not yet succeeded in giving a sufficiently clear and complete explanation of this process. Recently Burch et al. have published a review examining this kind of activation of C–H bonds in saturated hydrocarbons [9].

The interactions of methane on metal oxides have been explored by several authors [2,3,8]. The relationship between the different crystal planes of MoO_3 and their contribution to the activity and selectivity of catalytic reactions is important because it provides important information needed for the identification of active sites in this catalyst [10,11]. Molybdenum trioxide is an active and selective catalyst for the partial oxidation of alcohols and hydrocarbons [12–14]. In addition, MoO_3 based catalysts are widely studied for methane oxidation [15–20].

Focusing on the theoretical approaches, the extended Hückel (EH) method has been employed by several authors in order to study the hydrocarbon molecule interactions on metal oxide surfaces. Sambeth et al. used this formalism to explain the catalytic oxidation of methanol on V_2O_5 [21]. Rahmouni and Barbier studied the chemisorption of methanol on various faces of MoO_3 by EH calculations [12].

The calculations of Mehandru et al. drew important conclusions concerning the dissociative chemisorption of methane on MoO_3 surfaces in presence of O^- species. The results obtained using the atomic superposition and electron delocalization molecular orbital theory (ASED-MO) and a $Mo_3O_{11}^{-4}$ cluster show that O^- strongly activates C–H bonds. The presence of O^- was explained in terms of an UV O2p → Mo4d charge-transfer excitation. Heterolytic adsorption is most likely at edge sites and CH_3^- forms a donation bond to Mo^{+6}. If a homolytic pathway is followed, the products obtained at edge sites are less stable. In the same paper the authors mention the possibility that some methyl radicals could escape to the basal plane and

dimerize subsequently in ethane or, in presence of additional electron–hole pair excitations, to produce formaldehyde. In addition, the barrier to methyl radical diffusion over O^{-2} sites is approximately the same as the desorption energy, 0.4 eV. Finally, they propose that the homolytic adsorption at O^{-} sites on the basal planes will also take place, forming ethane and formaldehyde. Unless CH_2O is desorbed, additional electron–hole pair excitations should lead to further dehydrogenation and surface reduction with the formation of CO and CO_2 [22].

The goal of the present work is to perform a theoretical study of the dehydrogenation and subsequent oxidation of methane on different catalytic sites of a MoO_3 (100) surface. To this purpose a semi-empirical molecular orbital technique was employed, which will be described in Section 2.

2. Theoretical method

The computational technique used in this study is the ASED method developed by Anderson et al., which can be view as a modification of the EH theory [23–25]. One important improvement is the inclusion of a pair-wise repulsion term, based on the Hellmann–Feynman force theorem. This repulsive term allows the determination of equilibrium geometries for the adsorbed species. The diagonal elements of the Hamiltonian are taken as the negative valence orbital ionization potentials (IP). While the off-diagonal elements on the same center are zero, the off-diagonal elements on different centers are the average of the corresponding diagonal elements multiplied by: $S_{ij}\exp(-0.13R)$, where S_{ij} is the corresponding valence orbital overlap integral and R is the internuclear distance. This multiplicative factor can be considered to give an improved EH Hamiltonian in comparison with the Wolfsberg–Helmholtz formulation [26].

The atomic parameters used for this work, IP and Slater exponents, are those reported by Anderson et al. [27]. Regarding the atomic basis set, a full valence s + p + d Slater type was employed. All these parameters are listed in Table 1.

The calculation of the adsorption energy (ΔE_{total}) was performed as the difference between the total energy of the system when the adsorbed species/molecular fragments are at a finite distance from the surface, and the same energy when those species are far away from the solid surface. That is, the adsorption energy was calculated as:

$$\Delta E_{\text{total}} = E_{\text{total}}(\text{ads. species/metal oxide}) - E_{\text{total}}(\text{ads. species}) - E_{\text{total}}(\text{metal oxide})$$

The adsorbed species include CH_4, CH_3, CH_2, CH, C, H, CO, CH_2O and CO_2.

Table 1
Parameters for ASED-MO calculations

Atom	Orbital	Ionization potential (eV)	Slater exponent (au^{-1})	Linear coefficient	Electronegativity (Pauling)
Mo	4d	10.06	4.542	0.5899	1.8
			1.901	0.5899	
	5s	9.10	2.256		
	5p	5.92	1.956		
O	2s	26.48	1.946		3.5
	2p	11.62	1.927		
C	2s	15.59	1.5536		2.5
	2p	10.26	1.4508		
H	1s	13.60	1.0000		2.1

The ASED, being a useful improvement of the EH method, gives approximate results when calculations for molecular properties are compared to Hartree–Fock (HF) or configuration interaction (CI) results. Particularly, for those properties of transition-metal diatomic oxides such as equilibrium force constants, equilibrium bond lengths and bond dissociation energies, the ASED method brings satisfactory predictions [28–31]. It must be underlined to the reader that the reported energy values should be interpreted in their qualitative sense, due to the approximated nature of both the method and model.

Since several structural and geometrical aspects of the model must be considered at the same time, including adsorption site, azimuthal orientation, tilt angle, bond distortions and height above the cluster surface, certain assumptions were made. The criteria for exploring the mentioned characteristics of the systems and the structure of the clusters is described in Section 3.

3. The cluster model and the structure of the adsorption sites

In the last years several authors have reported the pronounced influence of the geometric features of oxide crystallites on the selectivity of oxidation reactions. Many studies have been devoted to understand the behavior of different MoO_3 crystal faces [12–14,18,19,32].

Rahmouni and Barbier, in a recent work, studied the interactions of CH_3OH with α-MoO_3 and found that the stability of the molecular chemisorption complexes increased as they pass from the (100) face to the (001) and (010) ones [12]. Tatiboüet and Germain studied the catalytic anisotropy of MoO_3 in the conversion of methanol [13]. The effect of ions geometric arrangement on the reactivity of adsorbed hydrocarbon molecules at different MoO_3 crystal planes was discussed by Ziólkowski for some catalytic reactions on the basis of the bond-length–bond-strength concept. According to this approach three types of surface oxygen atoms can be distinguished: (i) tightly bound inactive lattice oxygen atoms, (ii) weakly bound active lattice oxygen atoms and (iii) weakly bound active adsorbed oxygen atoms [14].

Smith and Ozkan studied the partial oxidation of methane to formaldehyde over MoO_3 samples exposing different relative amounts of (010) and (100) plane areas. The experimental characterization studies suggest that the O=Mo sites could be promoting the formation of formaldehyde, while the bridging sites Mo–O–Mo were more likely to lead to complete oxidation [18,19]. Brückman et al. studied the role of active sites on molybdate catalysts for olefin oxidation reactions [32].

In the following we will describe our cluster model. MoO_3 crystallizes in the orthorhombic system, with $a = 3.963$ Å, $b = 13.855$ Å and $c = 3.696$ Å. The space group is Pbnm [33]. The stereochemistry of the metal atom in MoO_3 can be best considered as that of a markedly distorted octahedron, although it can be easily deduced from the MoO_3 tetrahedron as a basic unit.

MoO_3 has a layer structure in which each layer is built up of MoO_6 octahedrons at two levels, connected along the *z*-axis by common edges and corners, so as to form zigzag rows and along *x*-axis by common corners only [2]. Moreover each layer exhibits, in the direction of *z*-axis, oxygen atoms which are common for three different octahedrons. Each octahedron also shares, along *x*-axis, two oxygen atoms with two neighboring octahedrons.

Besides, for each MoO_6 octahedron there is only one oxygen atom which is doubly bounded to the molybdenum atom (O=Mo). It occupies different positions along the *y*-axis. For each MoO_6 octahedron at the higher level this oxygen atom points up. On the contrary, for each MoO_6 octahedron at the lower level this oxygen atom points down.

The structure of the MoO_6 octahedron is shown in Fig. 1a. In addition, the MoO_3 cluster used in our calculations, considering the struc-

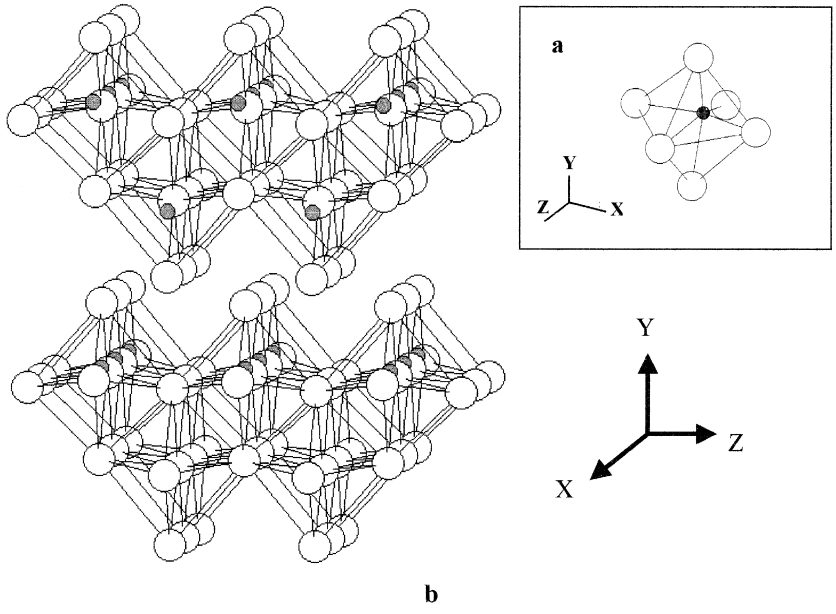

Fig. 1. (a) The MoO_6 octahedron structure and (b) superimposable cluster $Mo_{30}O_{107}^{-34}$ used in our calculations. (shaded circles) Mo, (open circles) O.

tural features above mentioned, is shown in Fig. 1b. It has 137 atoms distributed in two layers of 71 and 66 atoms each.

The idealized arrangement of molybdenum and oxygen atoms on the (100) plane of MoO_3 is shown in Fig. 2. The clean (100) plane presents coordinately unsaturated Mo^{+6} ions with one bridging O^{-2} ion missing from their coordination sphere. Thus it acquires the formal uncompensated charge $(+1)$. This plane also contains unsaturated bridging O^{-2} ions with one Mo^{+6} missing and a formal uncompensated charge of (-1) [2].

In order to model the (100) surface of MoO_3 the calculations were performed using a bulk superimposable $Mo_{30}O_{107}^{-34}$ cluster. This surface is formed by a perpendicular cleavage to the layers. The excess electrons assigned to the cluster, making it formally to bear a charge of (-34), serve to assure that all oxygen anions were in the (-2) oxidation state. This (-34) charge does not affect the evaluation of the electronic Hamiltonian matrix elements under the standard extended Hückel calculations. The usual procedure of dangling bonds saturation with hydrogen atoms did not improve the calculations in the present case.

To find the local energy minimum of each molecular fragment bond distances and interbond angles were optimized varying only the x, y and z atomic coordinates (in 0.1 Å steps). The sign of the energy gradient determined the

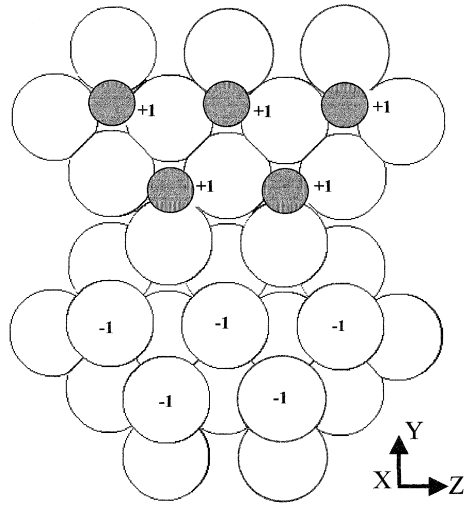

Fig. 2. Space fill idealised (100) MoO_3 face. The uncompensated charges are also shown. (shaded circles) Mo, (open circles) O.

next step direction. For each sequence the reaction coordinate was determined at approximately 0.3 Å steps. The same number of steps were used for all reaction sequences. We must underline that the reaction coordinate involves several geometric changes such as stretching, rotation and translation as it will be clarified later.

4. Results and discussion

The different processes explored in this work such as H-abstraction and CH_2O, CO and CO_2 formation, will be described in Sections 4.1, 4.2 and 4.3.

4.1. H-abstraction

4.1.1. CH_4–MoO_3 interaction on the layer exposing oxygen atoms

$CH_4 \rightarrow CH_3 + H$: As can be seen in Fig. 3, the methane adsorption is calculated to be unfavorable on this layer. The CH_4 approach to the surface produces a considerable energetic barrier. The abstracted H was positioned on a terminal oxygen atom (O=Mo) and a weak bond was found between the methyl group and the another oxygen atom. The system increases its energy by 1.8 eV. This sequence is shown in Fig. 4. Here the final C–O distance from the CH_3 fragment to the 'surface' O atom is equal to 4.0 Å while the distance from the H atom to the O=Mo site is equal to 1.15 Å. The CH_3-fragment adopts a sp^3 hybridization with one of the tetrahedral axes through the C atom oriented perpendicularly to the oxide surface.

The reported values were obtained optimizing simultaneously both H and CH_3 fragments. After that, the CH_3 group maintained the same geometry (< HCH angle = 109.5° and C–H distance = 1.32 Å) as in the free methane molecule (calculated with the atomic parameters reported in Table 1).

$CH_3 \rightarrow CH_2 + H$: This sequence is shown in

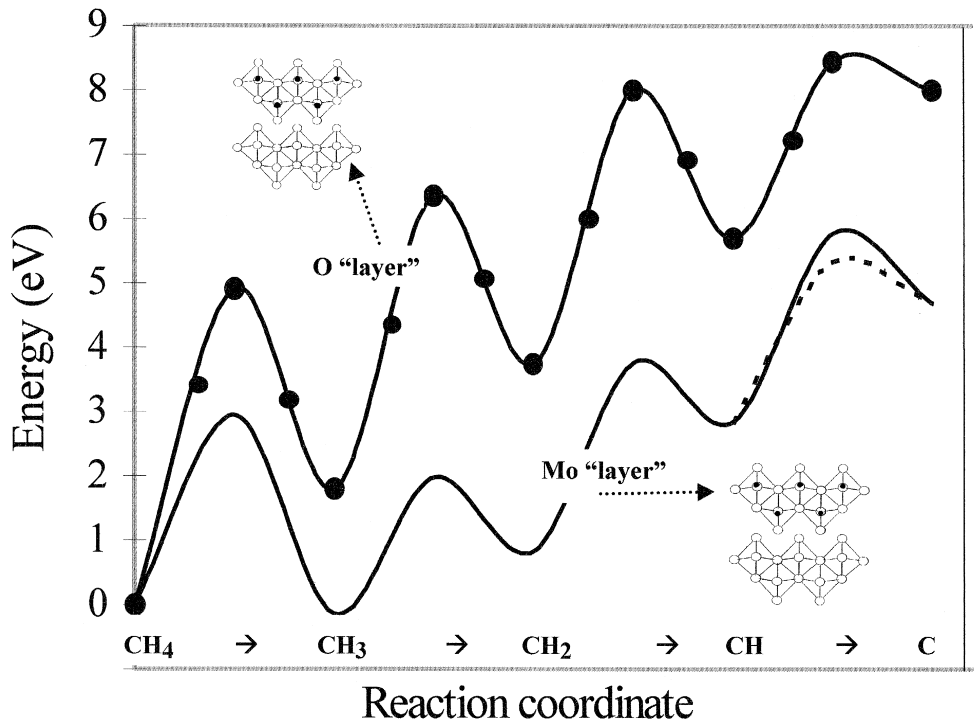

Fig. 3. Total energy curve versus reaction coordinate for H-abstraction. (————) Reaction over the layer exposing Mo atoms, (– ● –) reaction over the layer exposing O atoms and (– – –) fourth H abstraction, second alternative.

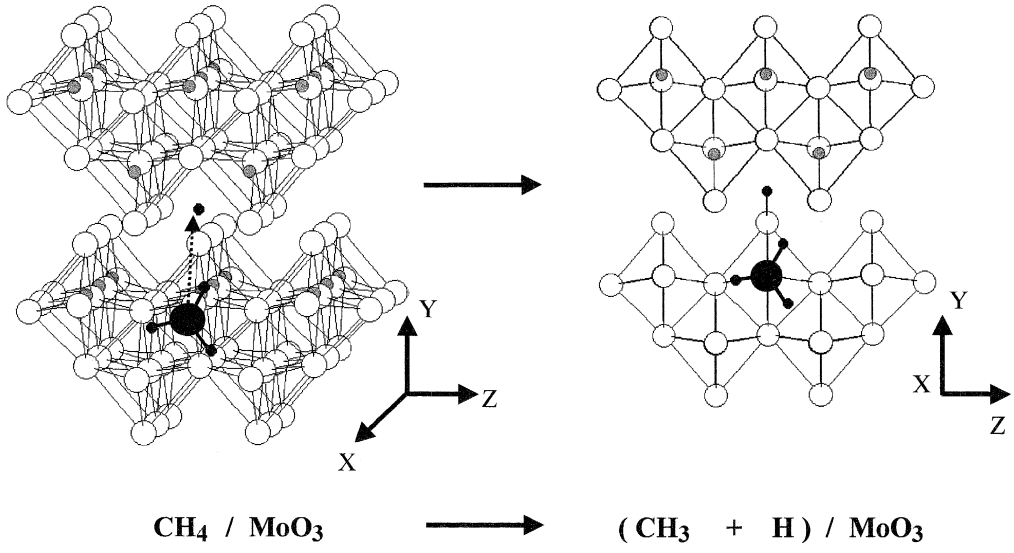

Fig. 4. Pathway for the first H-abstraction over the layer exposing O atoms. (small filled circles) H, (○) O, (shaded circles) Mo, (●) C.

Fig. 5. The H–O distance obtained was 1.1 Å while the methylene < HCH angles and C–H distances did not change after their optimization. The energy is increased by 1.94 eV (E_{total} = 3.74 eV) and the energy barrier results in 93% of the former (see Fig. 3).

$CH_2 \rightarrow CH + H$: The optimized H–O and C–O distances and the energy increment for the third H abstraction seem to be similar to the previous ones. The energy barrier results in 86% of the one in the first H-abstraction (see Fig. 3). This sequence is presented in Fig. 6.

$CH \rightarrow C + H$: As it was described in the previous cases, the H–O and C–O distances were optimized, obtaining a shorter C–O distance (2.17 Å, see Fig. 7). The energy increment for the last H abstraction is 2.3 eV, while the energy barrier results in 55% of the first H-abstraction barrier (see Fig. 3).

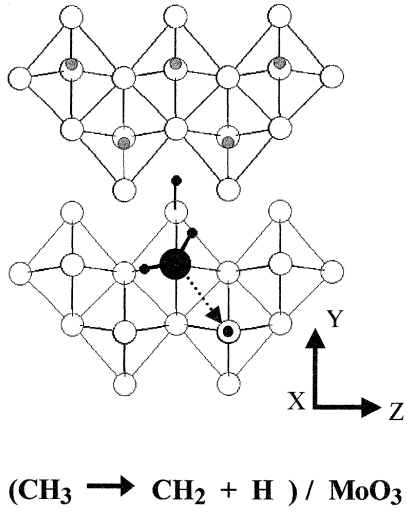

Fig. 5. Pathway for the second H-abstraction over the layer exposing O atoms. (small filled circles) H, (○) O, (shaded circles) Mo, (●) C.

4.1.2. CH_4–MoO_3 interaction on the layer exposing molybdenum atoms

$CH_4 \rightarrow CH_3 + H$: The first hydrogen to be abstracted was sent to an O atom double coordinated to a Mo atom (i.e. an O=Mo bond) in a similar way as it was described by Mehandru et al. [22]. The C–H bond breakage requires 3.2 eV in the vacuum (this value was calculated using the atomic parameters of the present work). Over the Mo layer the energy barrier results to be 2.95 eV high and the H–O distance of 1.1 Å. The methyl group bonded to the Mo atom was placed at a distance of 2.16 Å. The adsorption turned out more favorable (0.15 eV) with respect to free methane. The H charge results to be +0.16, while the CH_3 charge is

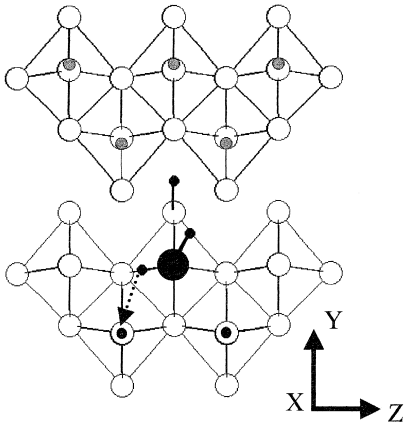

Fig. 6. Pathway for the third H-abstraction over the layer exposing O atoms. The initial and final site for the 3rd H are shown in the same figure. (small filled circles) H, (○) O, (shaded circles) Mo, (●) C.

−0.40. These values show the same tendency of fragments polarization than those obtained by Mehandru et al. [22] (+0.3 and −0.33, respectively) for the heterolytic scission. As in both calculations a non-self-consistent method was used, the concrete values of atomic charges must be considered only in a qualitative sense. The most important contribution to H_3C–Mo bond comes from the hybrid between the end orbital of CH_3 and the dz^2 orbital of Mo atom. This molecular orbital is above the O_{2p} band and comes out to be the HOMO orbital (Ref. [22]). Due to an H → O electron charge transfer being present, the overall charge balance assures that a fraction of these electrons is retained by the CH_3–Mo bond. Then CH_3 becomes somewhat negative charged.

The bond angles and optimized distances are indicated in Fig. 8. The < HCH bond angles and C–H distances of the CH_3 fragment resulted in 109.5° and 1.32 Å, respectively, as in the free molecule.

$CH_3 \rightarrow CH_2 + H$: The abstraction of the second hydrogen turned out into a barrier of 72% of the former. The energy increment for this sequence is 0.84 eV (see Fig. 3). In Fig. 9 the bond angles and optimized distances of CH_2 fragment are shown. The C–H distances are maintained at 1.32 Å.

$CH_2 \rightarrow CH + H$: This sequence presents a barrier higher than that corresponding to the second hydrogen abstraction, although its magnitude is similar to that of the first abstraction. The optimized bond angles and distances are indicated in Fig. 10.

$CH \rightarrow C + H$: Two possibilities were analyzed for the fourth H-abstraction (see Fig. 11a), starting from the situation shown in Fig. 10. In the first (Fig. 11b), the H atom was turned round the C atom and was abstracted with a 2.93 eV energy barrier. The system reaches a

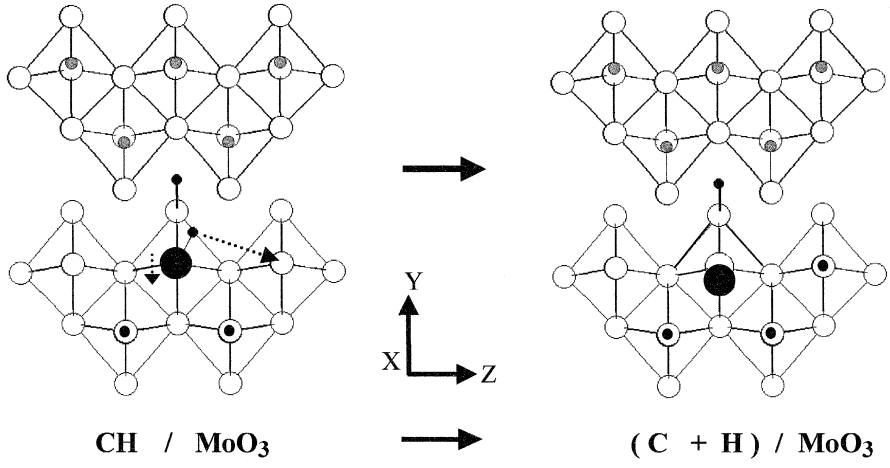

Fig. 7. Pathway for the fourth H-abstraction over the layer exposing O atoms. (small filled circles) H, (○) O, (shaded circles) Mo, (●) C.

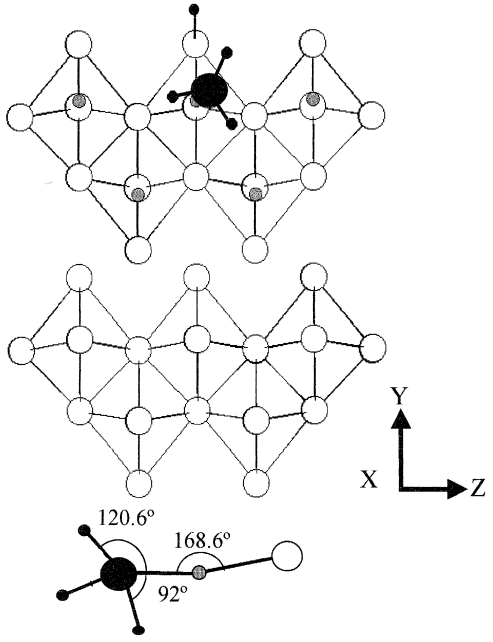

(CH_4 → CH_3 + H) / MoO_3

Fig. 8. Pathway for the first H-abstraction over the layer exposing Mo atoms. (small filled circles) H, (○) O, (shaded circles) Mo, (●) C.

total energy of 4.68 eV. In the second case, an adsorbed H atom from the previous sequence was moved as indicated in Fig. 11c with a barrier of 1.1 eV. This movement was proposed to generate a free O atom as an alternative adsorption site for the fourth H atom. For the latter proposal the total energetic barrier results to be 2.49 eV. The energy versus reaction coordinate plot for all the sequences is displayed in Fig. 3.

4.1.3. CH_4–MoO_3 interaction on the layers exposing molybdenum and oxygen atoms

The C–H bond breaking in the CH_3 fragment adsorbed over Mo atom (Fig. 8), demands 2.1 eV (see Fig. 3). A similar energetic value is necessary to desorb CH_3. Therefore, two different alternatives were explored:

(1) Starting from a desorption step and a translational displacement on the (100) plane, the 'free' CH_3 fragment could be readsorbed at an O atom of the other layer (see Fig. 4, right), obtaining in this way an additional stability of 0.13 eV. Furthermore, when the CH_3 fragment is in the 'vacuum' the H atoms could easily turn round the C atom. So, it comes to be possible for the CH_3 fragment to be readsorbed in a different geometry leading to H atoms closer to surface O atom. Nevertheless, our results indicate that the last sequence is unfavorable.

(2) Losing another H atom and giving rise to the CH_2–Mo species (Fig. 9), as Section 4.1.2) ($CH_3 \rightarrow CH_2 + H$).

Looking at the different adiabatic energy curves in Fig. 3 we can infer that the integral H-abstraction process for the three cases (Sections 4.1.1 and 4.1.2 and this section) we considered is essentially endothermic. Notably this same behavior has been obtained experimentally for the C–H bond rupture of free CH_4 and theoretically for CH_4 on La_2O_3 [34].

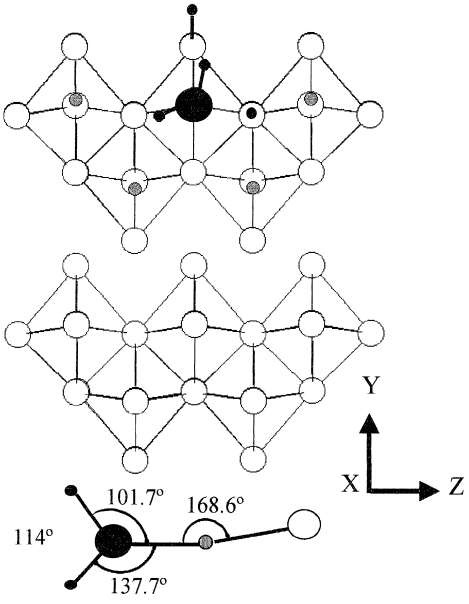

(CH_3 → CH_2 + H) / MoO_3

Fig. 9. Pathway for the second H-abstraction over the layer exposing Mo atoms. (small filled circles) H, (○) O, (shaded circles) Mo, (●) C.

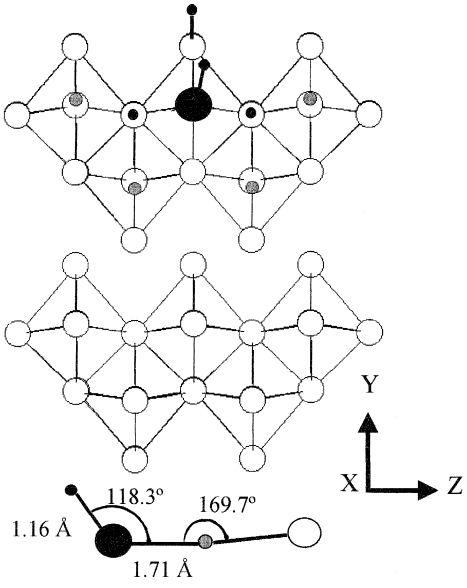

Fig. 10. Pathway for the third H-abstraction over the layer exposing Mo atoms. (small filled circles) H, (○) O, (shaded circles) Mo, (●) C.

Moreover the results of Fig. 3 clearly show that the heterolytic H-abstraction is an energetically more favorable process. Indeed the activation energy for the first homolytic H atom rupture and the final corresponding dissociated state are nearly 2 eV above those of the heterolytic abstraction. The subsequent stationary points for the homolytic process are more than 4 eV above those of the other mechanism.

The present results indicate that despite an important energy barrier being necessary for the first C–H bond activation, the overall oxidation process is kinetically more favored in the heterolytic mechanism. On the other hand ab-initio calculations performed for CH_4 on Al_2O_3 and La_2O_3 have shown an important barrier for CH_4 activation (of nearly 2 eV) [34]. Actual catalysts for complete oxidation work at elevated temperatures and hence this first activation barrier would be easily surmounted.

In a recent paper Yoshizawa et al. have analyzed using an ab-initio technique the possible reaction pathways for the conversion of methane to methanol catalyzed by FeO^+. The preferred mechanism includes an insertion intermediate $H–O–Fe^+–CH_3$. These authors conclude that the activation of hydrocarbons through the ferryl oxygen ($FeO–CH_4$) is unlikely because it does not correspond to a minimum or saddle point of the potential energy surface [35].

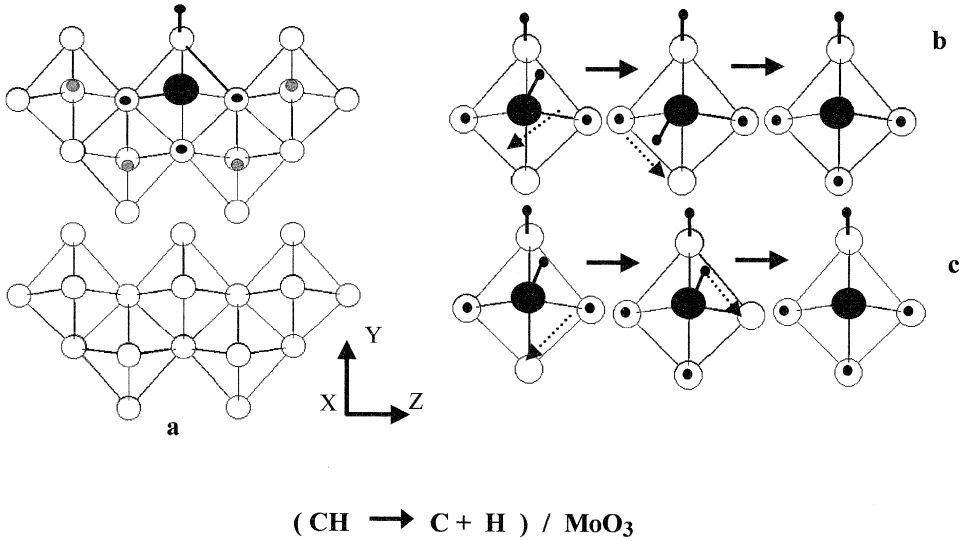

Fig. 11. (a) Final geometry after the fourth H-abstraction over the layer exposing Mo atoms. (small filled circles) H, (○) O, (shaded circles) Mo, (●) C. (b) Schematic movement for an H atom round the C atom. (c) Schematic movement for an adsorbed H atom.

Finally, we want to mention the EH calculations of CH_3OH chemisorption performed by Rahmouni and Barbier. These authors obtained for the heterolytic dissociation of methanal a surface ($CH_3O + H$) complex where the CH_3O group interacts with an unsaturated Mo atom of the surface [12]. This complex is more than 1 eV more stable than our $CH_3 + H$ complex. This result is reasonable taking into account the greater affinity of Mo to O atoms in order to fill its bulk coordination.

4.2. Formaldehyde formation

After the second H atom abstraction from methane three sequences are analyzed:

(a) Starting from CH_2–$O_{surface}$ species on the layer exposing O atoms.

(b) Starting from CH_2–$Mo_{surface}$ species on the layer exposing Mo atoms.

(c) A combination of steps from (a) and (b).

The CH_2O optimization was performed using the EH parameters above mentioned. While the bond angles so obtained are similar to the experimental reported values the interatomic distances result in 1.64 Å and 1.20 Å for C–H and C–O, respectively, which are rather long with respect to the experimental findings. Using larger H Slater exponents, slightly better distances are computed (~ 0.1–0.2 Å shorter). We think however that by using another set of EH parameters, the main results of general character we obtained would not undergo significant modifications, particularly considering our comparisons with the calculations of Mehandru et al. also performed within the ASED formalism [22]. The sequences (a)–(c) are discussed as follows:

(a) In Fig. 12 a, the CH_2O formation sequence is presented. This path included the desorption step and a bond angle and distances rearrangement with respect to the optimized free formaldehyde. The final state is positioned 1.14 eV above the starting point. Comparing the formaldehyde formation with the third H abstraction process, a decrease of 0.79 eV in the activation barrier can be observed. The resulting CH_2O species is 0.82 eV more stable than that obtained after the third H abstraction (see Fig. 13).

(b) In Fig. 9 the starting point can be observed. Interactions with neighboring oxygen atoms of different coordinations are also analyzed. Fig. 12b shows the oxygen atoms labeled **1**, **2**, **3** and **4**. In Table 2 the most energetically

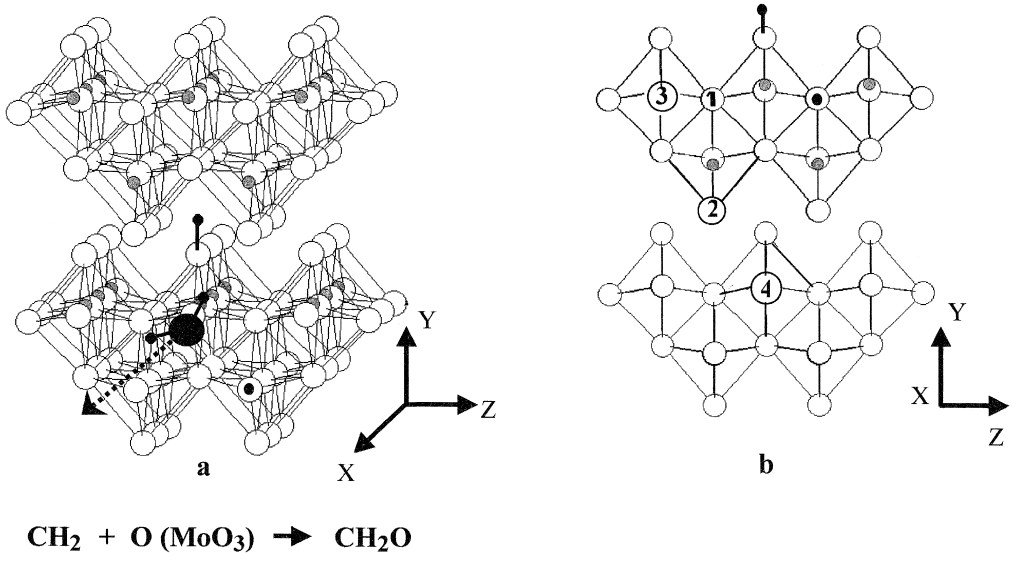

Fig. 12. (a) Formaldehyde formation sequence on the O exposing layer. The desorption is done following $x(100)$-axis. (b) Oxygen atoms **1**, **2**, **3**, **4** (see also Table 2).

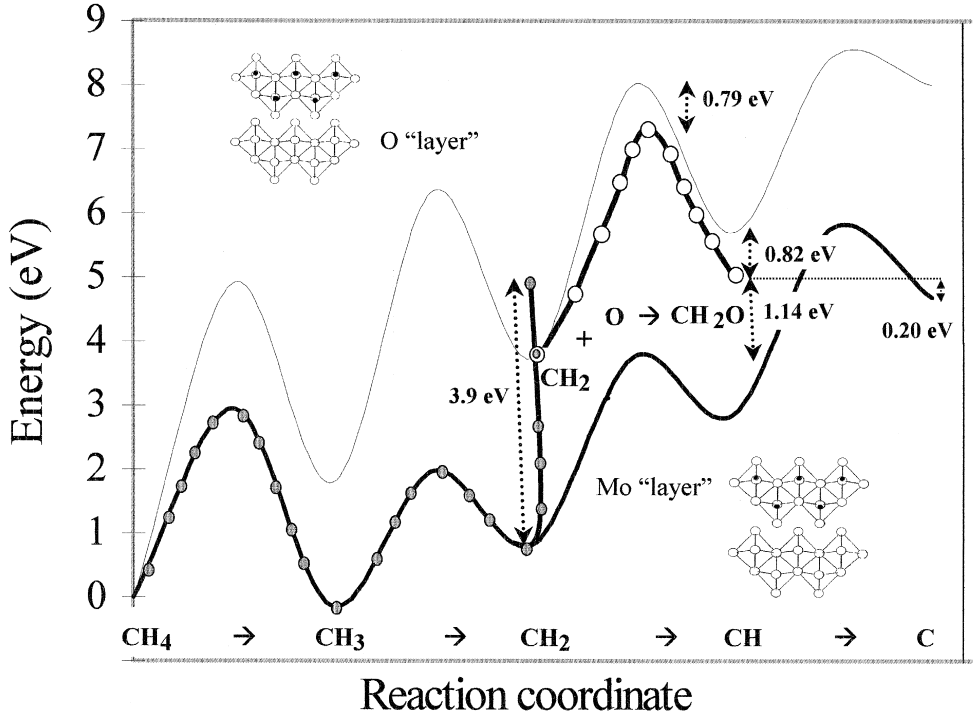

Fig. 13. Total energy curve versus reaction co-ordinate for formaldehyde formation. (– ∘ –) Sequence according to Fig. 12a on the O exposing layer; (– · –) sequence with combination of steps on O and Mo layers. The methane oxidation sequences are also shown on (————) Mo and (————) O.

favorable situation can be observed, which corresponds to oxygen atom **4** (surface). For oxygen atoms **1** and **2** the coordination is referred to the number of bonded Mo atoms, while oxygen atom **3** simulates an adsorbed O atom.

(c) An alternative path could be developed starting with the desorption of the fragment adsorbed to the Mo atom (see Fig. 9) and followed by its adsorption to the oxygen atom **4**. This step has a 3.9 eV energy barrier (see Fig. 13). The process would continue with the CH_2O desorption, as indicated in (a). Among the different hypothesis studied here, the last seems to be the most favorable. In Fig. 13 it can also be observed that the CH_2O formation process just described comes out only 0.20 eV less favorable than the complete H-abstraction process over the layer exposing Mo atoms (leading to a final adsorption energy value of 4.68 eV, see Fig. 3).

Table 2
Relative energies for CH_2–Mo + O interactions

Oxygen type	Relative adsorption energy
1 (3-coordinate)	1.63
2 (1-coordinate)	1.88
3 (adsorbed)	1.77
4 (surface)	1.00

4.3. CO and CO_2 formation

The CO formation performed after the sequence described in Section 4.1.2 (over the layer exposing Mo atoms) is a highly unfavorable mechanism when it is compared to a similar process over the layer exposing oxygen atoms (see Section 4.1.1).

Taking into account the situation shown in Fig. 7 (where the C–O bond distance is of 2.17 Å) the CO molecule formed after passing a 0.45 eV barrier results to be 1.78 eV more stable than at the starting point. The CO molecule

formation sequence involves the approach of the neighboring O atom to the C atom up to a distance of 1.2 Å. After that, the CO fragment is desorbed from the cluster, leaving four adsorbed H atoms and an oxygen vacancy.

Finally, because of its availability of O sites the possible formation of CO_2 over the layer exposing oxygen atoms was studied. Among several explored alternatives, the one which results to be the most favored in order to form CO_2 involves the simultaneous approximation of two O atoms to the C atom, which is finally desorbed as CO_2. Nevertheless, even for this sequence, the energetic barrier involved is excessively high when compared with any of the other barriers reported in this present work.

5. Conclusions

The aim of the present work was to analyze theoretically different alternative pathways for CH_4 adsorption–oxidation on MoO_3 (100). The analysis was based on calculation of the adsorption energy of the system by molecular orbital calculations (ASED).

The theoretical study of the CH_4–MoO_3 chemical interaction suggests that while the H-abstraction requires less energy for each consecutive step the overall process remains endothermical. The different sequences and sites for hydrogen abstraction from methane, analyzed over different layers exposing molybdenum and oxygen atoms, allowed us to conclude that the heterolytic H-abstraction is an energetically more favorable process in comparison to the homolytic one.

Regarding the oxygenated products, both CO and CH_2O are possible to be formed from lattice oxygen and dehydrogenated methane. In the first case, the activation barrier is of 0.45 eV with a stable final state, while the CH_2O species is almost 1 eV more stable than those obtained after the third H atom abstraction from methane.

No matter which surface or paths were considered the CO_2 formation involving lattice oxygen results to be the most unfavorable processes studied.

Our results are in good qualitative agreement with ab-initio SCF-MO calculation on oxide surfaces [34] and other EH calculations [12,22] performed to study the reactivity of the MoO_3 surface.

Acknowledgements

This work was partially supported by Fundación Antorchas, CONICET (Argentina) and a direct research grant from Departamento de Física, UNS. The authors acknowledge the help of Ing. S. Gesari in elucidating the MoO_3 crystal structure.

References

[1] R. Pitchai, K. Klier, Catal. Rev. Sci. Eng. 28 (1986) 13.
[2] A. Bielanski, J. Haber, Oxygen in Catalysis, Chemical Industries, vol. 43, M. Dekker, New York.
[3] Z. Zhang, X.E. Verykios, M. Baerns, Catal. Rev. Sci. Eng. 36 (3) (1994) 507.
[4] V.D. Sokolosvskii, E.A. Mamedov, Catal. Today 14 (1992) 331.
[5] T. Ito, J.H. Lunsford, Nature 314 (1985) 721.
[6] D.J. Discroll, W. Martir, J.X. Wang, J.H. Lunsford, J. Am. Chem. Soc. 107 (1985) 58.
[7] V.D. Sokolosvskii, G.M. Aliev, O.V. Buyesvskaya, A.A. Davydov, Catal. Today 4 (1989) 293.
[8] V.D. Sokolosvskii, O.V. Buyevskaya, S.M. Aliev, A.A. Davydov, in: G. Centi, F. Trifiro (eds.), New Developments in Selective Oxidation, Elsevier, Amsterdam, 1990.
[9] R. Burch, M.J. Hayes, J. Mol. Catal. A 100 (1995) 13.
[10] A. Michalak, K. Hermann, M. Witko, Surf. Sci. 366 (1996) 323.
[11] A. Papakondylis, P. Sautet, J. Phys. Chem. 100 (1996) 10681.
[12] A. Rahmouni, C. Barbier, J. Mol. Struct. 330 (1995) 359.
[13] M.T. Tatibouet, J.E. Germain, J. Catal. 76 (1982) 238.
[14] J. Ziólkowski, J. Catal. 80 (1983) 263.
[15] H.F. Liu, R.S. Liu, D.J. Liew, R.E. Johnson, J.H. Lunsford, J. Am. Chem. Soc. 106 (1984) 4117.
[16] M.M. Khan, G.A. Somorjai, J. Catal. 91 (1985) 263.
[17] N.D. Spencer, C.J. Pereira, R.K. Grasselli, J. Catal. 126 (1990) 546.
[18] M.R. Smith, U.S. Ozkan, J. Catal. 141 (1993) 124.
[19] M.R. Smith, U.S. Ozkan, J. Catal. 142 (1993) 226.
[20] S. Pack, M.P. Rosynek, J.H. Lunsford, J. Phys. Chem. 98 (1994) 11786.

[21] J. Sambeth, A. Juan, L. Gambaro, H. Thomas, J. Mol. Catal. 118 (1997) 283.
[22] S.P. Mehandru, A.B. Anderson, J.F. Brazdil, R.K. Grasselli, J. Phys. Chem. 91 (1987) 2930.
[23] A.B. Anderson, J. Chem. Phys. 62 (1985) 1187.
[24] A.B. Anderson, R.W. Grimes, Y. Hong Sung, J. Phys. Chem. 91 (1987) 4245.
[25] A.B. Anderson, J. Electroanal. Chem. 280 (1990) 37.
[26] M. Wolfsberg, L. Helmholtz, J. Chem. Phys. 20 (1952) 837.
[27] A.B. Anderson, Y. Kim, D.W. Ewing, R.K. Grasselli, M. Tenhover, Surf. Sci 134 (1983) 237.
[28] A.B. Anderson, R.W. Grimes, Y.H. Sung, J. Phys. Chem. 91 (1987) 4245.
[29] A.B. Anderson, S.Y. Hongand, J.L. Smialek, J. Phys. Chem. 91 (1987) 4250.
[30] M.A. Stiakaki, A.C. Tsipis, C.A. Tsipis, C. Xanthopoulos, Chem. Phys. 189 (1994) 535.
[31] E.G. Bakalbassis, M.A. Stiakaki, C.A. Tsipis, C.A. Tsipis, Chem. Phys. 205 (1996) 389.
[32] K. Brückman, J. Haber, J. Catal. 106 (1987) 188.
[33] L. Kihlborg, Arkiv Kemi 21 (1963) 357.
[34] M.J. Capitan, J.A. Odriozola, A. Marquez, J. Fernandez Sanz, J. Catal. 156 (1995) 273.
[35] K. Yoshizawa, Y. Shiota, T. Yamabe, Chem. Eur. J. 3 (1997) 1160.